Key Engineering Materials Vols. 198-199 (2001) pp 179-202
© (2001) Trans Tech Publications, Switzerland
doi:10.4028/www.scientific.net/KEM.198-199.179

Laser Microtexturing of Implant Surfaces for Enhanced Tissue Integration

John L. Ricci[1] and Harold Alexander[2]

[1] Department of Orthodontics, New Jersey Dental School, University of Medicine and Dentistry of New Jersey, 110 Bergen Street, Newark NJ 07103-2400, USA

[2] Orthogen Corporation, Springfield NJ, USA

Keywords: Laser Microtexturing, Implant Surfaces, Tissue Integration

Introduction. The success or failure of bone and soft tissue-fixed medical devices, such as dental and orthopaedic implants, depends on a complex combination of biological and mechanical factors. These factors are intimately associated with the interface between the implant surface and the surrounding tissue, and are largely determined by the composition, surface chemistry, and surface microgeometry of the implant. The relative contributions of these factors are difficult to assess. This study addresses the contribution of surface microtexture, on a controlled level, to tissue integration.

All rights reserved. No part of contents of this paper may be reproduced or transmitted in any form or by any means without the written permission of TTP, www.ttp.net. (ID: 207.201.200.66-23/05/11,17:14:07)

In vitro and in vivo experiments have demonstrated the role of surface microgeometry in tissue-implant surface interaction although no well-defined relationship has been established. The general relationship, as demonstrated by in vivo experiments on metallic and ceramic implants [1-10] indicates that smooth surfaces promote formation of thick fibrous tissue encapsulation and rough surfaces promote thinner soft tissue encapsulation and more intimate bone integration. Smooth and porous titanium surfaces have also been shown to have different effects on the orientation of fibrous tissue cells in vitro [11,12]. Surface roughness has been shown to be a factor in tissue integration of implants with hydroxyapatite surfaces [4, 8], and to alter cell attachment and growth on polymer surfaces roughened by hydrolytic etching [13]. Roughened surfaces have also shown pronounced effects on differentiation and regulatory factor production of bone cells in vitro [14-16]. Defined surface microgeometries, such as grooved and machined metals and polymer surfaces [11, 17-20] have been shown to cause cell and ECM orientation in vivo and can be used to encourage or impede epithelial downgrowth in experimental dental implants [9]. Surface texturing has also been shown to adhere fibrin clot matrix more effectively than smooth surfaces [21], forming a more stable interface during the collagenous matrix contracture that occurs during healing. This is an effect which may be important in determining early events in tissue integration.

Textured surfaces influence the tissue/implant interface on tissue, cellular, and molecular levels. On a most basic (tissue) level these surfaces have higher surface areas than smooth surfaces and interdigitate with tissue in such a way as to create a more stable mechanical interface. As noted they also have significant effects on cell function, and on a molecular level they promote adhesion of early wound healing components. We have observed that, in the short term, fibrous tissue cells form an earlier and more organized collagenous capsule at smooth interfaces than at textured interfaces. This suggests that textured surfaces have an additional advantage over smooth surfaces. They inhibit colonization by fibroblastic cell types that arrive early in wound healing and encapsulate smooth substrates [22].

It has long been an accepted practice to roughen or texture regions of implants to encourage bone integration and produce smooth regions to promote soft tissue integration. The upper region (collar) of dental implants are often left in an "as machined" or sometimes a polished state to encourage gingival attachment [23] and prevent plaque formation, which favors more roughened surfaces [24]. Several techniques are commonly used to produce texturing. These include machining, surface blasting, and acid etching. These techniques produce a range of surface microstructures of varying sizes and shapes, from sub-micron to more than 50 μm in size. None of these techniques allow micron-tolerance control of microstructure size, and placement, and blast texturing, which is usually produced using glass bead for matte finishes and alumina grit for surface roughening, can cause significant surface contamination with embedded fragments of blast medium [25, 26]. Newer blast methods use resorbable or soluble blast medium to avoid this problem. Blasting is often followed by acid etching, which removes the embedded material and produces a fine microtexture of its own. Acid etching is also used alone to produce fine microtexturing.

In this paper we will describe the common machined, blasted, and etched surfaces used on dental and orthopaedic implants, and describe the development and testing of a series of new laser micromachined surfaces for use on these implants. In previous in vitro experiments [22] we have investigated (1) the effects of textured surfaces on colony formation by fibroblasts, and (2) the effects of controlled surface microgeometries on fibroblast colonization. Based on these results we have designed, fabricated, and tested laser microgrooved surfaces with features in specific size ranges, which are applied using computer-controlled laser ablation techniques. We have tested these on titanium alloy and commercially-pure titanium implants in in vivo models. These experimental surfaces have highly-organized and oriented microstructures. They can be produced with features in specific size ranges, and can be applied to specific, highly controlled areas of implants. The results suggest that controlled surface microgeometry, in specific size ranges, can enhance bone and soft tissue integration and control the local microstructural geometry of attached tissue. These surfaces are currently being applied to dental implants and tested in human clinical studies.

Materials and Methods.

Experimental Surface Production and Evaluation.

A series of textured metal samples were compared with regard to surface microstructure and composition. These included the machined surfaces of titanium alloy dental implants (mA), alumina grit blasted commercially-pure titanium (gCP), polished commercially-pure titanium (pCP), grit-blasted titanium alloy samples (gA), glass bead-blasted titanium alloy (bA), acid etched, glass bead-blasted titanium alloy (aA), and titanium alloy blasted with resorbable blast medium (RBM). These samples were not coated with carbon or gold-palladium as is often done for scanning electron microscopy. They were examined using either a JEOL JSM-T300 scanning electron microscope (SEM) equipped with a GW Electronics type 30A backscattered electron imaging system, and a Fisons/Kevex Delta Class IV x-ray microprobe system, or a Hitachi S-2500 scanning electron microscope with a GW backscattered electron imaging system and a Princeton Gamma Tech IMIX x-ray microprobe system. In all cases the scanning electron microscope (SEM) was used to examine surface microstructure, the backscattered electron imaging system was used to identify the presence of embedded surface contamination, and the x-ray microprobe system was used to evaluate the composition of these embedded surface contaminants.

Fabrication of Laser Micromachined Implants. Microgroove patterns were produced on flat and cylindrical commercially-pure titanium and titanium alloy specimens. These were produced using a pulsed, computer-controlled Excimer laser system and large-area masking techniques. In early studies the samples were produced using a block pattern approach. A block-shaped area of the surface, corresponding to the area covered by the large-area mask, was pulse-ablated until the desired depth was reached. Then the sample was moved and another area was pulse ablated. In later

cylindrical dental implant specimens a continuous system was used in which the sample was rotated while the laser continuously pulse-ablated to produce a continuous pattern. Two types of microgrooved surfaces were produced. The most extensively used surface had 12 μm wide microgrooves and ridges between grooves. The grooves had 12 μm depth. These were referred to as MG12 surfaces. An additional MG8 surface was produced in later experiments. This surface had 8 μm wide grooves and ridges, and 4 μm depth grooves. The sizes of these structures were selected based on earlier cell culture experiments [22].

After fabrication, all samples were cleaned using organic solvents, sonicated in detergent solution, and passivated in nitric acid according to industry standard ASTM protocols, before autoclave sterilization and implantation.

In Vivo Studies. Two models; an implantable chamber system and an intramedullary rod model, were used to text bone response to laser microtextured implants.

The Implantable Chamber System used in this study has been described in other publications and used to test a number of materials including other textured metal surfaces, hydroxyapatite surfaces, polymer surfaces, and resorbable polymer materials [10, 27-28]. This system was designed to evaluate bone and soft tissue response to experimental materials. In this method we surgically placed two experimental chambers in each canine. Each chamber contained 10 test specimens and was implanted in a bone window cut in the distal lateral femur. This system allowed testing of bone and soft tissue response to up to 20 experimental samples in each canine. The experimental implant chamber system was used to compare bone response to the MG12, gA, and gCP surfaces. These three surfaces were also produced with preset coatings of medical grade calcium sulfate cement for testing in the same experiment. Calcium sulfate has been shown to dissolve in the body and stimulate bone formation [29]. These samples were designated MG12/CS, gA/CS, and gCP/CS. Twelve skeletally mature large canines were used in this study and 120 samples were tested at 3, 6, and 12 weeks.

Canine Intramedullary Rod Model. A canine intramedullary (IM) rod model was also used to test cylindrical specimens of the MG12 (produced in circumferential and longitudinal orientations) and gCP surfaces, as well as the polished commercially pure titanium (pCP). Each IM rod consisted of a central mounting rod and six stacked cylinders containing the test surfaces. Each rod was placed in the intramedullary canal of an intact femur (no fracture). These samples were surgically placed in the central third of the femur using an approach through the trochanteric fossa of the hip. In each animal two IM rods were placed, one in each femur. One rod contained the MG12 samples (both orientations) and the other contained the gCP and pCP specimens. Three animals (six rods, 36 specimens) were used in this study. This model was used to examine longer-term response to these experimental surfaces at 3 and 6 months.

Evaluation of Tissue Response.

Faxitron Histomorphometry of Bone Penetration. Faxitron high-resolution x-ray images were used to document bone ingrowth into the implantable chambers. These images of the intact chambers showed the furthest extent of bone penetration into each channel. This method shows a profile of the bone growing into the channels and the films were used to quantitate the maximum extent of bone penetration. These x-ray films were digitized using a Wild M3C stereomicroscope equipped with a Dage-MTI CCD72 high-

resolution videocamera attached to a personal computer equipped with a PixelPipeline frame-acquisition board, and BDS-Oncor image acquisition/analysis software.

The channels, lined by the experimental surfaces and showing bone penetration, were measured end-to-end to determine accurate channel length, and the center of the channel was determined. The furthest extent of bone penetration, from each open end of the channel, was then measured for each channel. Each bone penetration measurement was divided by the distance to the center of the channel. Thus, a measurement of 100% represented full bone penetration from one opening of the channel to the center. Two 100% measurements for one channel meant that bone penetrated the channel from end-to-end.

Tensile Mechanical Testing of the Bone/Implant Interface. Mechanical evaluation was conducted on samples from the chamber model study in order to examine the tensile strength of attachment of ingrown bone to the various surfaces in the study. Each sample consisted of a pair of 7 x 8 mm plates of the experimental materials and the ingrown bone and soft tissue, which formed a 1 x 5 x 8 mm sample between the plates. This "sandwich" was tested in tensile mode to failure in an Instron servohydraulic mechanical testing system by applying tensile force to the top and bottom plates.

The test system consisted of two flat, parallel, attachment surfaces fixed to the servohydraulic actuator and to the load cell. The sample was placed on the lower surface (attached to the load cell) and its lower plate was cemented in place with a small amount of cyanoacrylate cement. The actuator was then lowered and cemented to the upper plate of the specimen. After both plates were cemented firmly the sample was tested in tension at a rate of 10% strain per minute (the crosshead speed was 0.10 mm/min. and the distance between the plates is 1.0 mm) until failure. Failure strength was measured in Newtons.

The cyanoacrylate cement was used because of its high tensile strength, short setting time, and its ability to set in the presence of moisture. Its use allowed rapid testing of fresh specimens without drying. Since the plates of the test specimen were held parallel in the precision-machined polyethylene chambers during bone penetration, they were fixed in parallel position by the ingrown, attached bone. Thus the plates of the removed samples remained rigidly parallel, and the testing was conducted with the plates in parallel orientation. Plate orientation was also routinely evaluated by faxitron imaging. Thus, precision chamber machining and assembly, and the use of precision test fixturing, were utilized to ensure parallel plate orientation during testing.

After testing, the failed specimens were removed from the test fixturing by shearing the plates from the test fixture surfaces, taking advantage of the relatively low shear strength of the cyanoacrylate cement.

In this model the interface tested represented the region between the 5 x 8 mm side of the tissue and the experimental surface. For reference, a 40-N force on this 40-mm^2 sample represented 1 MPa of failure stress if there was bone attachment along the entire interface.

Some samples in each group were saved intact for electron microscopy of the intact bone/implant interface. Some tested samples (with one intact interface remaining) were also processed for electron microscopy in order to examine the failed interface. This provided information on modes of failure.

Imaging of the Implant/Tissue Interface. Intact (untested) chamber model specimens, some mechanically-tested specimens (with one intact interface), and some samples from the IM rod model were dehydrated, embedded in polymethylmethacrylate, and sectioned. Some samples were processed for undecalcified histology while others were polished, and the surfaces were vapor-deposited with a 60 nm layer of carbon.

Some mechanically-tested chamber specimens and IM rod specimens were deproteinated for 30 minutes in 4% sodium hypochlorite (bleach) at pH 11 to remove soft tissue and expose bone mineral and metal structures. These samples were dehydrated, critical point dryed, and vapor-deposited with a 60 nm layer of carbon or sputter coated with a 60 nm layer of gold-palladium.

These samples were examined using a JEOL JSM-T300 scanning electron microscope (Tokyo) equipped with a GW Electronics (Norcross, GA) type 30A backscattered electron imaging system.

Statistical Analysis.

Comparison of all mean values in this study were conducted using Student's *t*-tests, with statistical significance defined as $p \leq 0.05$.

Results.

Description of Surface Microtextures. The surfaces evaluated by SEM showed microstructure in different size ranges. The mA surfaces showed oriented microstructures produced by machining (Fig. 1). These structures were in the sub-micron to 5μm range with relatively shallow depth. They were consistent with those reported in other studies [23] and are a very common surface on the collars of dental implants where soft tissue attachment is expected and plaque accumulation is to be avoided.

The bA surface shows surface microstructure produced in the sub-micron to 50μm range (Fig. 2). These surfaces show mechanical damage and gouging produced by the blasting technique. Figure 2 represents a backscattered electron image that shows the presence of embedded material of a darker gray scale range than the metal. This has been shown to be embedded blast debris [25, 26]. We have observed that some of this material is released from the surface after implantation [26] and represents a possibly significant source of inflammatory or abrasive debris. These surfaces, and similar alumina grit-blasted surfaces (like the gA and gCP surfaces), are commonly used on orthopaedic implants to encourage bone integration.

The acid-etched alloy surface (aA) shows non-oriented surface microstructure in the range of sub-micron to 50μm in size (Fig. 3) with extensive sub-micron pitting. Before acid etching this surface was similar to that shown in Fig. 2. The acid etching removes the embedded blast debris and generally produces a distribution of microstructure size that is smaller than that seen on the bA surface. This is a surface that is commonly used on the regions of dental implants that are expected to integrate with bone.

Figure 4 shows an RBM surface. This surface is produced by blasting with an abrasive that can easily be removed without acid etching. It shows non-oriented microstructure in the sub-micron to 50μm range, with similar microstructure to the bA surface.

Laser microgrooved surfaces were found to be reproducible and consistent. The surfaces showed small amounts of regional variation and could be produced in well

defined areas. Figure 5 shows a medium-power magnification scanning electron micrograph of a block-form MG12 surface produced on the 1 mm-wide collar of a prototype titanium alloy dental implant. The surface shows 12μm microgrooves and ridges. The grooves are relatively smooth while the ridges show sub-micron to 6μm structures produced by the accumulation of ablated material from the grooves. The block pattern production method produces discontinuities between blocks.

Figure 6 shows an MG12 surface produced on the 1mm collar of a dental implant by the continuous ablation method. Figure 7 shows a higher magnification of this surface. The grooves and ridges are more consistent, there are no discontinuities between regions, and the laser pulses produce small (less than 1μm) ridges in the depths of the grooves. Figure 8 shows an MG8 surface, which has similar microstructural characteristics to the MG12 surface, but has 8μm grooves and ridges, and 4μm depth.

In Vivo Studies.

Implantable Chamber and IM Rod Study Results. Implant chamber model studies showed that canine bone grew into channels lined with the microgrooved surfaces faster and more extensively than in channels lined with blast textured surfaces (Fig. 9). Calcium sulfate also encouraged rapid bone ingrowth with all surfaces [29], and the combination of the MG12 surface and calcium sulfate (MG12/CS) produced the most rapid and thorough bone ingrowth of all samples. The statistical differences between the MG12 and CS-coated surfaces, compared to the gA and gCP surfaces (uncoated) were significant at both time periods. Note that the microgrooves were oriented parallel to the direction of bone ingrowth. New bone was also observed to attach directly to the MG12 and MG12/CS surfaces (Fig. 10.) and the trabecular bone adjacent to these surfaces was strongly oriented parallel to the microgrooves (Fig. 11). This orientational effect of the MG12 surfaces on attached bone orientation was confirmed in the IM rod samples where orientation of attached bone trabeculae followed microgroove orientation whether it was circumferential or longitudinal (Figs. 11 and 12). Bone attachment to the MG12 and MG12/CS surfaces was strong enough to measure in tension (Fig. 13) and failed tensile-test specimens often showed bone left behind in the microgrooves. Bone surfaces exposed after implant removal always showed extensive bone attachment and growth into the microgrooves (Figs. 10, 11 and 14), with trabecular attachments spreading parallel to the microgrooves and blending together to form continuous bands. Electron microscopic results suggested that these surfaces caused orientation of attached cells (Fig. 14), which produced oriented extracellular matrix and oriented bone microstructure. This was not observed on textured surfaces or polished surfaces. Textured surfaces showed moderate direct bone attachment, that was not directional, and the polished surfaces showed little direct bone attachment and mostly fibrous encapsulation.

Proposed Surfaces for Control of Tissue Integration of Dental Implants. Based on the results of these experiments we are currently conducting feasibility studies of human tissue response to laser microgrooved dental implants. We have applied these microgrooved surfaces to the collar regions of dental implants in an attempt to control the organization and attachment of bone, soft tissue, and epithelium.

Discussion. Microtextures are commonly produced on metal surfaces to promote tissue integration. The standard methods used by the biomedical industry; machining, blasting, and acid-etching, showed varying microstructure sizes, distributions, and configurations. Some blast textured surfaces also showed extensive contamination by

embedded blast medium. Even though these textured surfaces are relatively uncontrolled with regard to microstructure size, shape, and distribution, they perform better than smooth surfaces with regard to bone integration. The results suggest that microstructure may be optimized through an understanding of the interaction between microstructure and tissue/cell/molecular interaction. We have attempted to develop a series of controlled microstructure surfaces, through laser modification techniques, that take advantage of the results of earlier in vitro and in vivo studies to design optimized surfaces for hard and soft tissue integration.

Our in vivo results suggest that the laser microgrooved surfaces represent a first stage improvement over existing surfaces. These results can probably be explained at the cellular level based partially on our results showing that fibroblast colonization is inhibited by these surfaces, and also by the results of others showing the effects of textured surfaces on bone cell differentiation [14-16]. Thus, on a cellular level microtextured surfaces may suppress early fibrous tissue encapsulation and enhance the differentiation of bone forming cells. These effects are probably partially based on the relationship between microgroove size and depth, and the ability of cells to attach, spread, and migrate. Suppression of cell spreading inhibits growth [30] and directs cell migration. Cell orientation and migration influence the microstructural production of extracellular matrix which results in oriented tissue production. These results are in agreement with in vitro studies showing that oriented bone cells produce oriented extracellular matrix [31]. Microtexturing of this type probably works on several levels since this type of surface would produce a mechanically stable interface and probably enhance early attachment of fibrin and other proteins [21]

Conclusions. We have surveyed currently used textured implant surfaces, and conducted earlier experiments on cell response to microstructure. Based on these results we have developed methods for production of laser-microtextured surfaces on metal implants. These methods produce surfaces that have significant advantages over existing industry standard surfaces. These methods produce clean, consistent microstructures, in highly-defined size ranges, on a micron scale, and can be used to place specific microtextures in highly defined areas. These microstructures can be produced in organized patterns that essentially microengineer the structure of adjacent tissue. These high-surface-area microtextures show excellent osseointegration and the ability to control the trabecular organization of adjacent bone. Early results suggest that they also control the microstructure of adjacent soft tissue. These engineered surfaces are currently being tested on dental implants with encouraging early results. They are also being developed for other biomedical applications.

This project was supported by grants from the Orthopaedic Research and Education Foundation, the New Jersey Center for Biomaterials through the New Jersey Commission on Science and Technology, NSF grant DMI-9304020, and NIH grant 1R41 NS351551-01 to Orthogen Corporation.

References.

1. Albrektsson T, Brånemark P-I, Hansson H-A, Lindström J: Osseointegrated titanium implants. Acta Orthop Scand 52:155-170, 1981.

2. Albrektsson T, Hansson H-A, Ivarsson B: Interface analysis of titanium and zirconium bone implants. Biomaterials 6:97-101, 1985.
3. Albrektsson T, Hansson H-A: An ultrastructural characterization of the interface between bone and sputtered titanium or stainless steel. Biomaterials 7:201-205, 1986.
4. Haddad RJ Jr, Cook SD, Thomas KA: Biological fixation of porous-coated implants. J Bone Joint Surg 69A:1459-1466, 1987.
5. Linder L, Albrektsson T, Brånemark P-I, Hansson HA, Ivarsson B, Jonsson U, Lundstrom I: Electron microscopic analysis of the bone-titanium interface. Acta Orthop Scand 54;45-52, 1983.
6. Linder L, Carlsson A, Marsal L, Bjurstein LM, Brånemark P-I: Clinical aspects of osteointegration in joint replacement: a histologic study of titanium implants. J Bone Joint Surg 70B:550-555, 1988.
7. Thomas KA, Cook SD: An evaluation of variables influencing implant fixation by direct bone apposition. J Biomed Mater Res 19:875-901, 1985.
8. Thomas KA, Kay JF, Cook SD, Jarcho M: The effect of surface macrotexture and hydroxylapatite coating on the mechanical strengths and histologic profiles of titanium implant materials. J Biomed Mater Res 21:1395-1414, 1987.
9. von Recum AF: Applications and failure modes of percutaneous devices: a review. J Biomed Mater Res 18:323:336, 1984.
10. Ricci JL, Spivak JM, Blumenthal NC, Alexander H: Modulation of Bone Ingrowth by Surface Chemistry and Roughness. In: The Bone-Biomaterial Interface, edited by JE Davies, University of Toronto Press, Toronto, Ont. Canada, pp. 334-349, 1991.
11. Chehroudi B, Gould TRL, Brunette DM: Effects of a grooved titanium-coated implant surface on epithelial cell behaviour in vitro and in vivo. J Biomed Mater Res 24:1067-1085, 1990.
12. Inoue T, Cox JE, Pilliar RM, Melcher AH: Effect of the surface geometry of smooth and porous-coated titanium alloy on the orientation of fibroblasts in vitro. J Biomed Mater Res 21:107-126, 1987.
13. McAuslan BR, Johnson C: Cell responses to biomaterials I: adhesion and growth of vascular endothelial cells on poly(hydroxyethyl methacrylate) following surface modification by hydrolytic etching. J Biomed Mater Res 21:921-935, 1987 .
14. Batzer R, Liu Y, Cochran DL, Szmuckler-Moncler S, Dean DD, Boyan BD, Schwartz Z: Prostaglandins mediate the effects of titanium surface roughness on MG63 osteoblast-like cells and alter cell responsiveness to 1 alpha,25- (OH)2D3. J Biomed Mater Res. 41(3)489-496, 1998.
15. Kieswetter K, Schwartz Z, Hummert TW, Cochran DL, Simpson J, Dean DD, Boyan BD: Surface roughness modulates the local production of growth factors and cytokines by osteoblast-like MG-63 cells. J Biomed Mater Res.32(1)55-63, 1996.
16. Lohmann CH, Sagun R, Sylvia VL, Cochran DL, Dean DD, Boyan BD, Schwartz Z: Surface roughness modulates the response of MG63 osteoblast-like cells to 1,25-(OH)(2)D(3) through regulation of phospholipase A(2) activity and activation of protein kinase A. J Biomed Mater Res 47(2): 139-51, 1999.
17. Brunette DM, Kenner GS, Gould TRL: Grooved titanium surfaces orient growth and migration from human gingival explants. J Dent Res 62:1045-1048, 1983.
18. Brunette DM: Fibroblasts on micromachined substrata orient hierarchically to grooves of different dimensions. Exp Cell Res 164:11-26, 1986.

19. Clark P, Connolly P, Curtis ASG Dow JAT, Wilkinson CDW: Topographical control of cell behavior. II. Multiple grooved substrata. Development 108:635-644, 1990.
20. den Braber ET, de Ruijter JE, Jansen JA: The effect of a subcutaneous silicone rubber implant with shallow surface microgrooves on the surrounding tissues in rabbits. J Biomed Mater Res.37(4)539-547, 1997.
21. Davies JE: Mechanisms of endosseous integration. Int J Prosthodont.11(5)391-401, 1998.
22. Ricci JL, Charvet J, Frenkel SR, Chang R, Nadkarni P, Turner J, Alexander H: Bone Response to Laser Microtextured Surfaces. In: Bone Engineering, edited by JE Davies, Em^2 Inc., Toronto, Ont. Canada, 2000.
23. Sawase T, Wennerberg A, Hallgren C, Miyamoto I, Albrektsson T: Atomic force microscopic study of commercially available implant abutments. Clin Implant Dent Rel Res 1(2):92-97, 1999.
24. Quirynen M, Marechal M, Busscher HJ, Weerkamp AH, Darius PL, van Steenberghe D: The influence of surface free energy and surface roughness on early plaque formation. An in vivo study in man. J Clin Periodontol 17:138-144, 1990.
25. Ricci JL, Kummer FJ, Alexander H, Casar RS: Embedded particulate contaminants in textured metal implant surfaces (Technical Note). J Applied Biomater 3(3):225-230, 1992.
26. Ricci JL, Kummer FJ, Scott D, Pedowitz D, Casar RS, Alexander H: Effects of texturing techniques on surface composition of metal orthopaedic implants. In: Surface Modification Techniques VII, ed TS Sudarshan. Insitute of Materials, London, 1994.
27. Spivak JM, Ricci JL, Blumenthal NC, Alexander H: A New Canine Model to Evaluate the Biological Response of Intramedullary Bone to Implant Materials and Surfaces. J Biomed Mater Res 24(9):1121-1149, 1990.
28. Choueka J, Charvet JL, Koval KJ, Alexander H, James KS, Hooper KA, Kohn J: Canine bone response to tyrosine-derived polycarbonates and poly(L-lactic acid). J Biomed Mater Res 31:35-41, 1996.
29. Ricci JL, Alexander H, Nadkarni P, Hawkins M, Turner J, Rosenblum S, Brezenoff L, DeLeonardis D, Pecora G: Biological mechanisms of calcium sulfate replacement by bone. In: Bone Engineering, edited by JE Davies, Em^2 Inc., Toronto, Ont. Canada. 2000.
30. Ingber DE, Madri JA, Folkman J: Endothelial growth factors and extracellular matrix regulate DNA synthesis through modulation of cell and nuclear expansion. In Vitro Cell Dev Biol:23(5)387-394, 1987.
31. Gomi K, Davies JE: Guided bone tissue elaboration by osteogenic cells in vitro. J Biomed Mater Res:27(4)429-31, 1993.

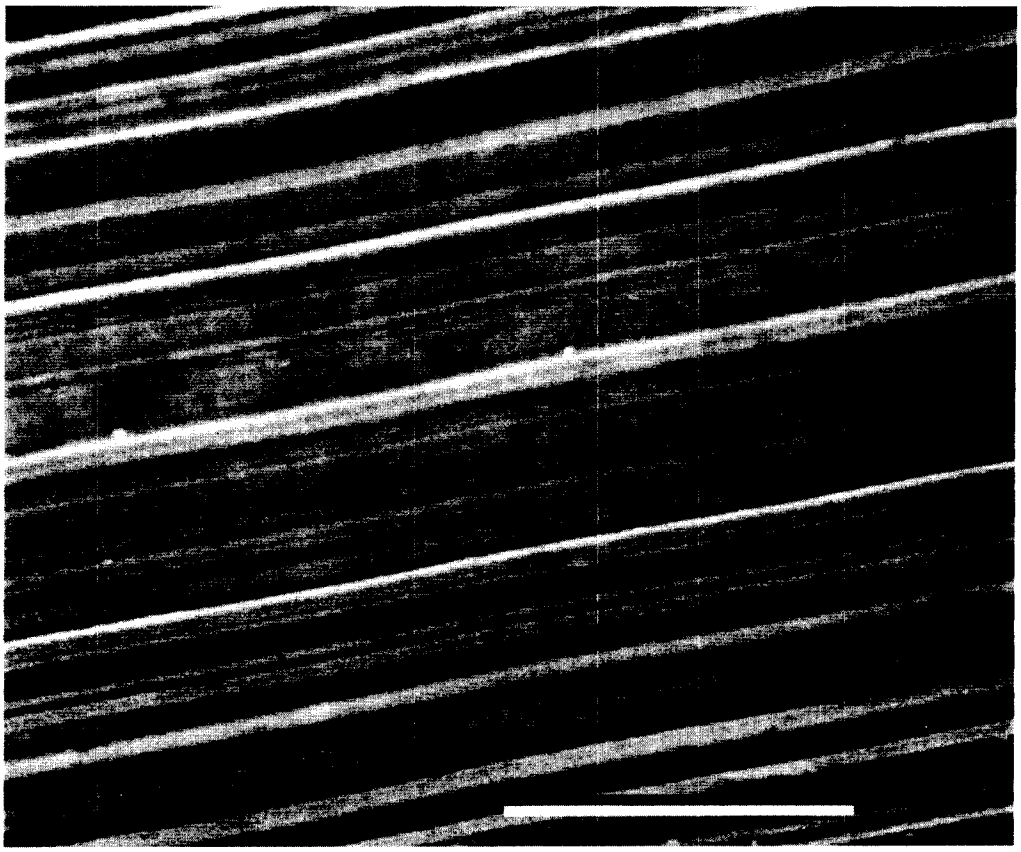

Figure 1. Medium power scanning electron micrograph of an mA surface showing small machining marks with little depth. Bar = 30μm.

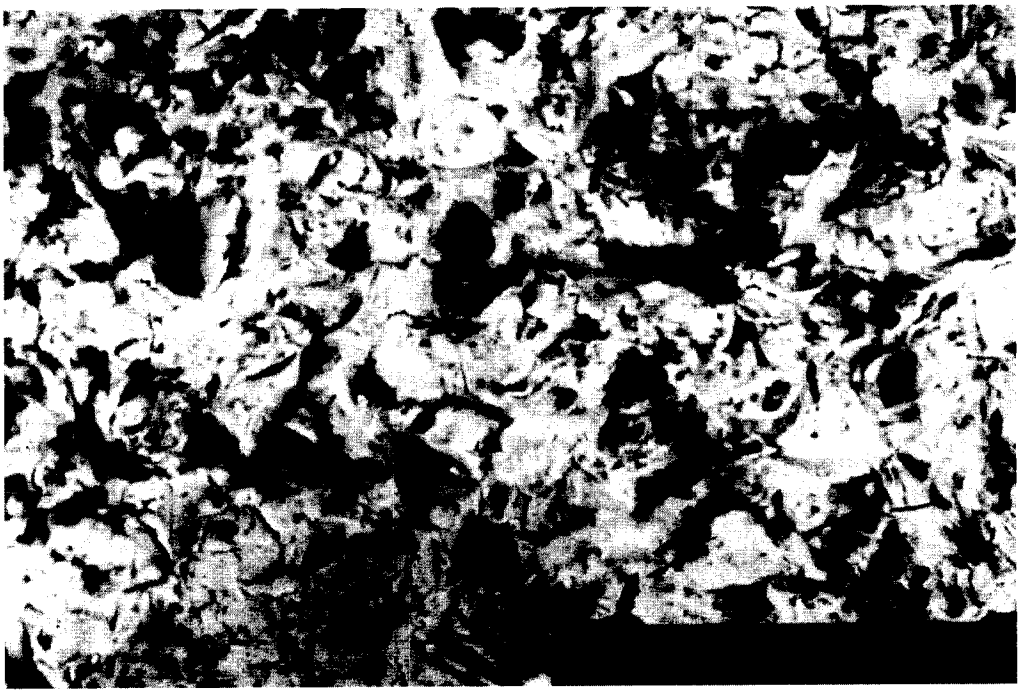

Figure 2. Medium power scanning electron micrograph (backscattered electron imaging mode) of a bA surface showing the blast-induced roughness and embedded blast residue as dark inclusions in the surface. Bar = 100μm.



Figure 3. Medium power scanning electron micrograph of an aA surface showing the fine microtexture produced by acid etching. Bar = 10μm.

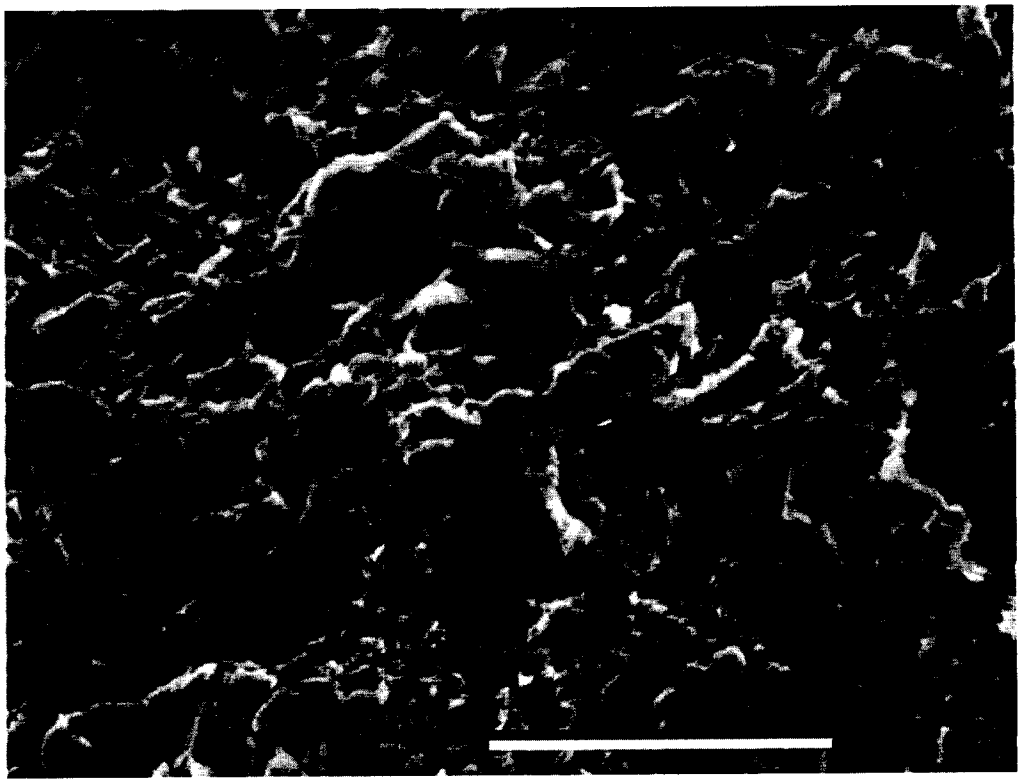

Figure 4. Medium power scanning electron micrograph of an RBM surface showing features similar to those shown in Fig. 2. There are no particles of blast debris embedded in the surface. Bar = 30μm.

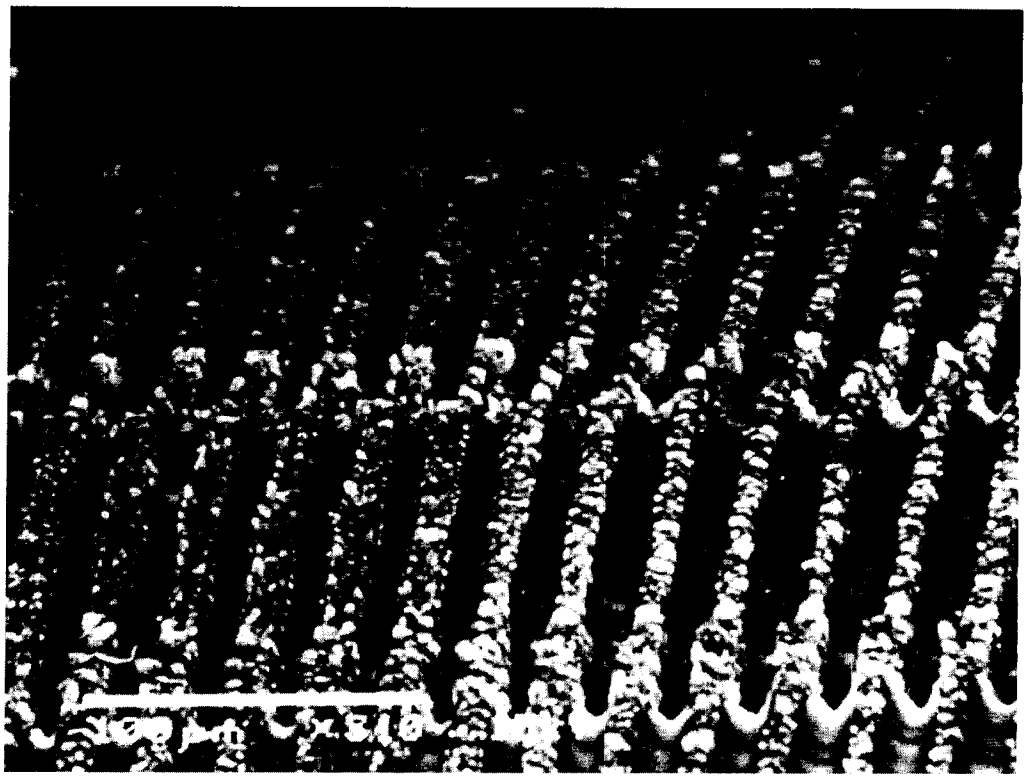

Figure 5. Medium power scanning electron micrograph of a prototype dental implant with the upper 1 mm of the collar microtextured with the MG12 surface. Bar = 100μm. (From Ricci et al., in Bone Engineering, ed. JE Davies, Em^2 Inc., Toronto, Ont. Canada, 2000, reprinted with permission.)

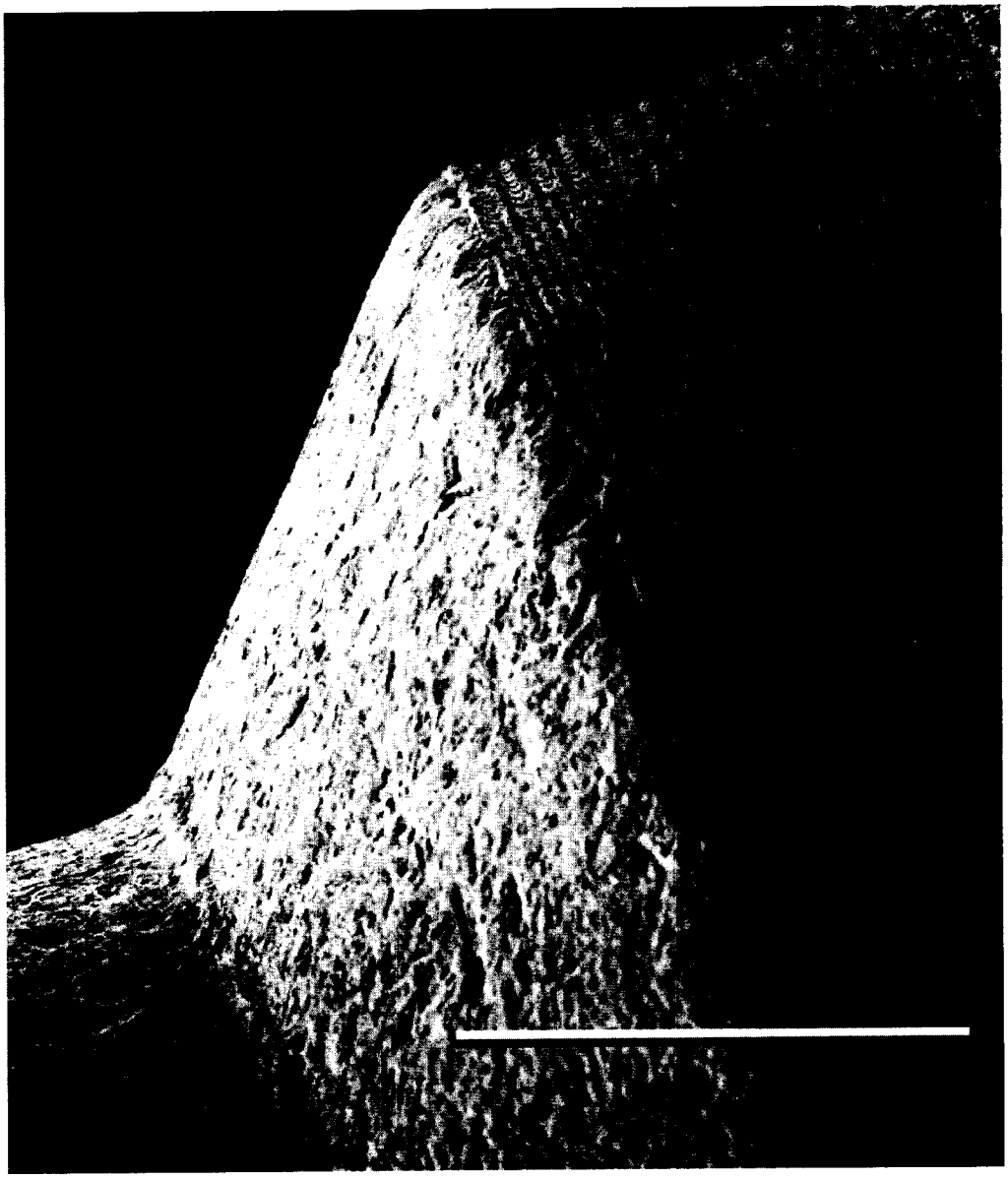

Fig. 6. Low magnification scanning electron micrograph of a prototype dental implant with the 1 mm collar (right) microtextured with the MG12 surface produced using a continuous ablation method. The remaining portion of the implant shows the RBM surface. Bar = 500μm.



Figure 7. Medium power scanning electron micrograph of a prototype dental implant with the MG12 surface produced by continuous ablation. Bar = 43μm.

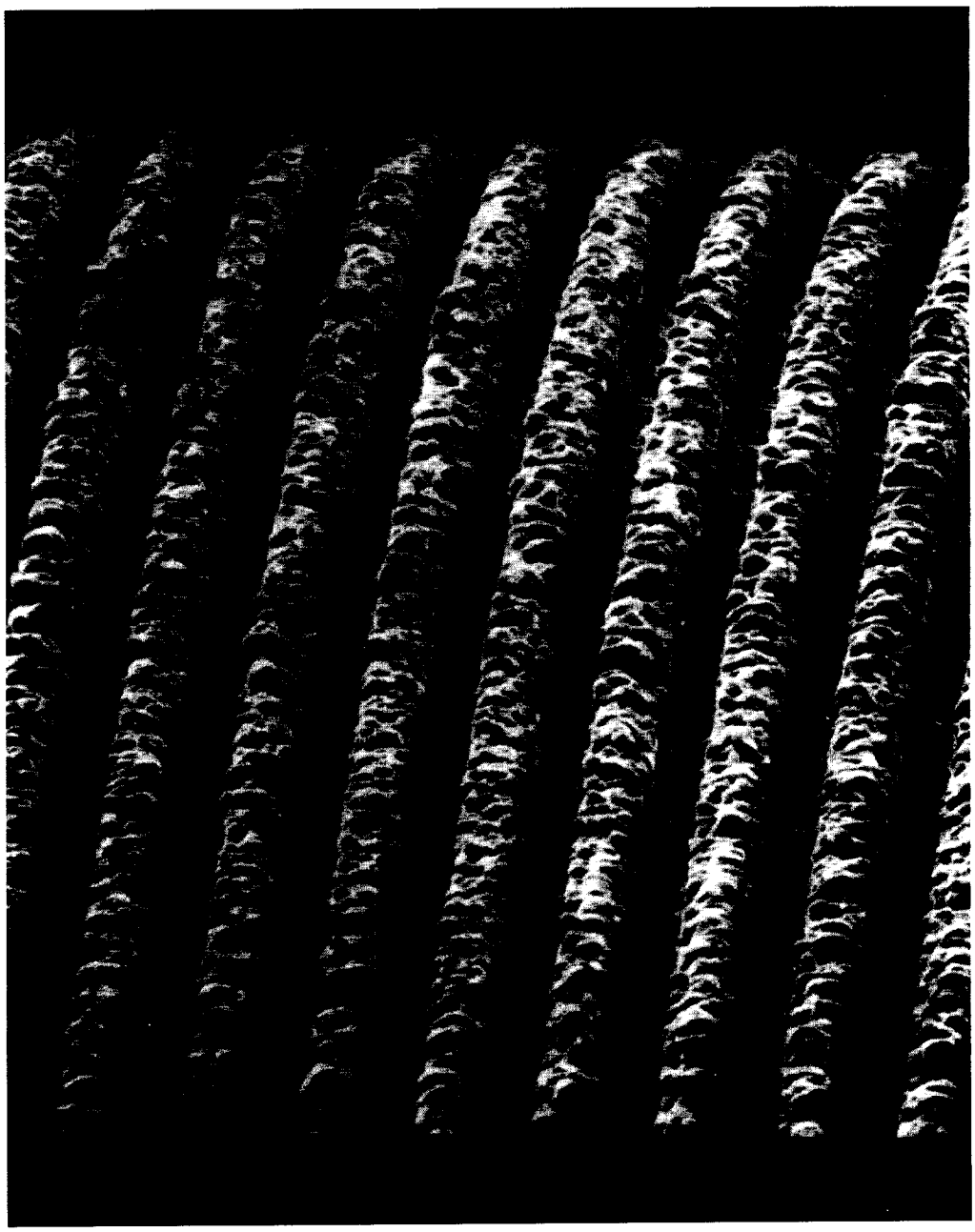

Figure 8. Medium power scanning electron micrograph of a prototype dental implant with the MG8 surface produced by continuous ablation. Bar = 43μm.

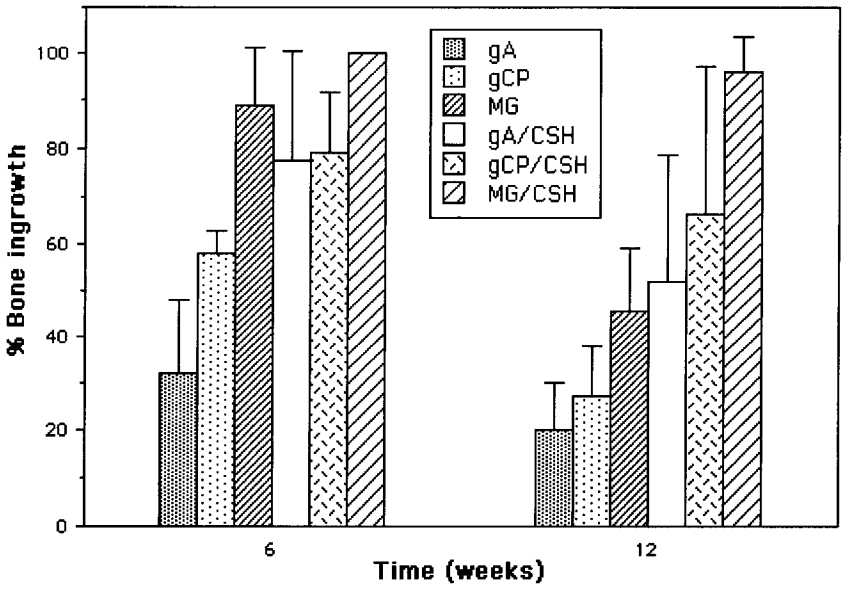

Figure 9. Graph of bone ingrowth into the implantable chamber showing the effects of the MG surfaces and the CS treatment. (From Ricci et al., in Bone Engineering, reprinted with permission.)

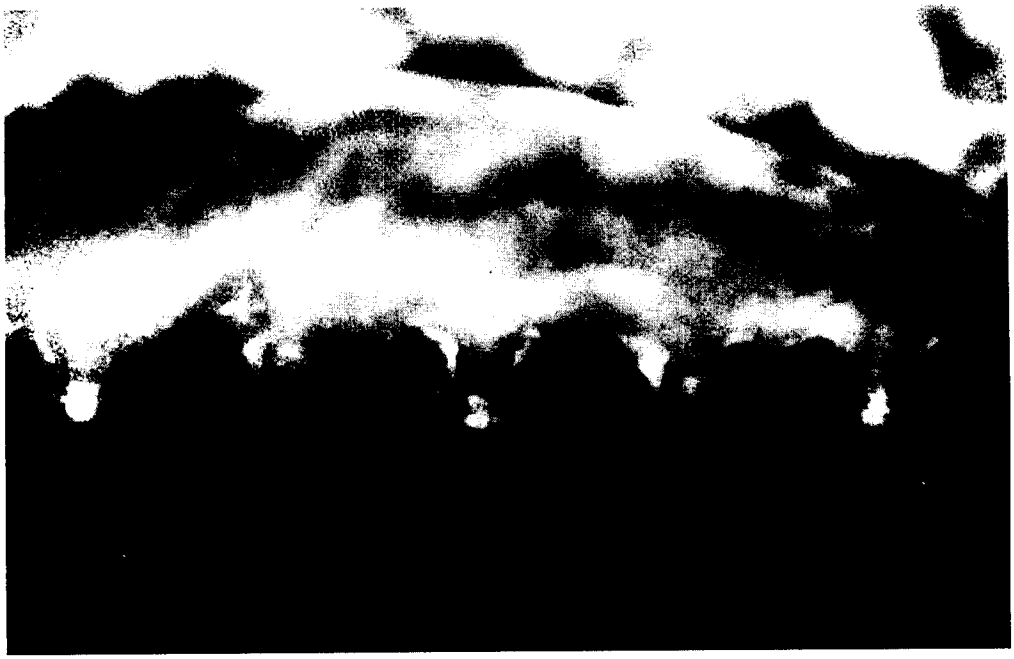

Figure 10. High power light photomicrograph of a bone sample adjacent to a MG12 surface. A small area of attached trabecular bone is shown. The bone has grown into the microgrooves of the surface. (From Ricci et al., in Bone Engineering, reprinted with permission.)

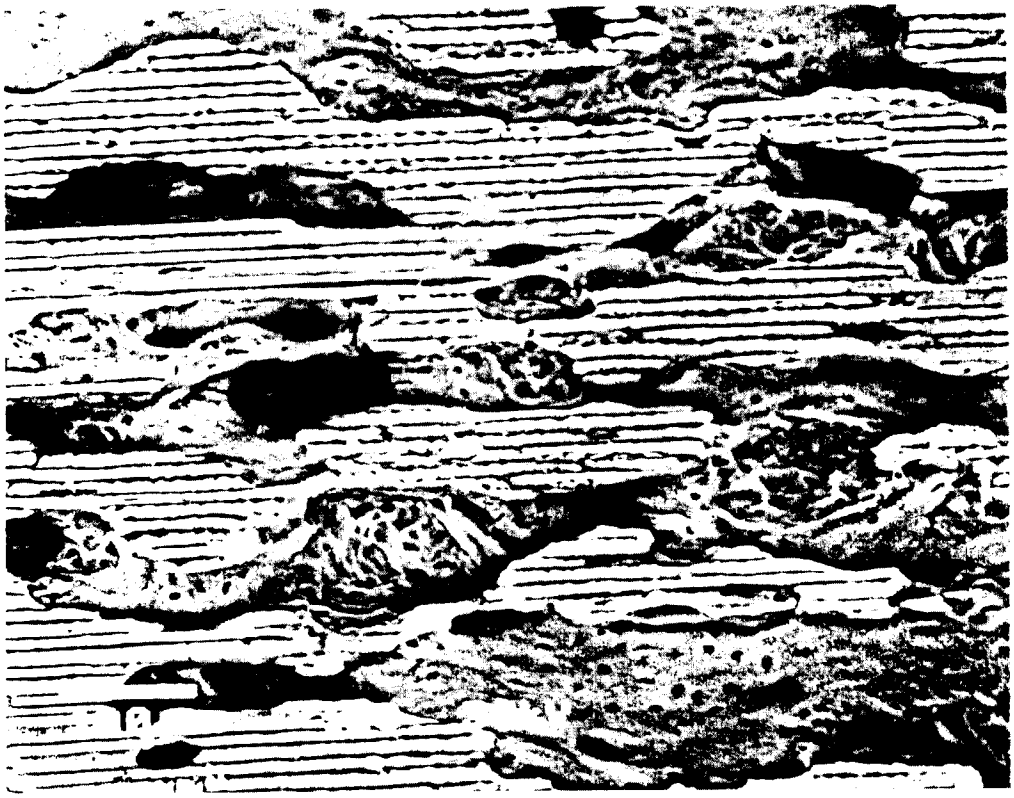

Figure 11. Medium power scanning electron micrograph of a deproteinated bone specimen from the IM rod study. The implant has been removed, and many areas of bone attachment to the surfaces are seen. Bone in these areas shows clear impressions of the implant surface and had grown into the microgrooves. The attachment areas are clearly oriented and elongated parallel to the microgrooves. Several attachments run together to form continuous bands. Bar = 100 μm. (From Ricci et al., in Bone Engineering, reprinted with permission.)



Figure 12. Low power scanning electron micrograph of a deproteinated bone specimen from the IM rod study. The implant has been removed, and many small areas of bone attachment to the surfaces are seen. The bone is oriented according to the microgrooving on the implant, which was oriented longitudinally (horizontal) on the right segment and circumferential on the left segment. A 300 μm seam with no microtexturing was in the center. Bar = 1000 μm. (From Ricci et al., in Bone Engineering, reprinted with permission.)

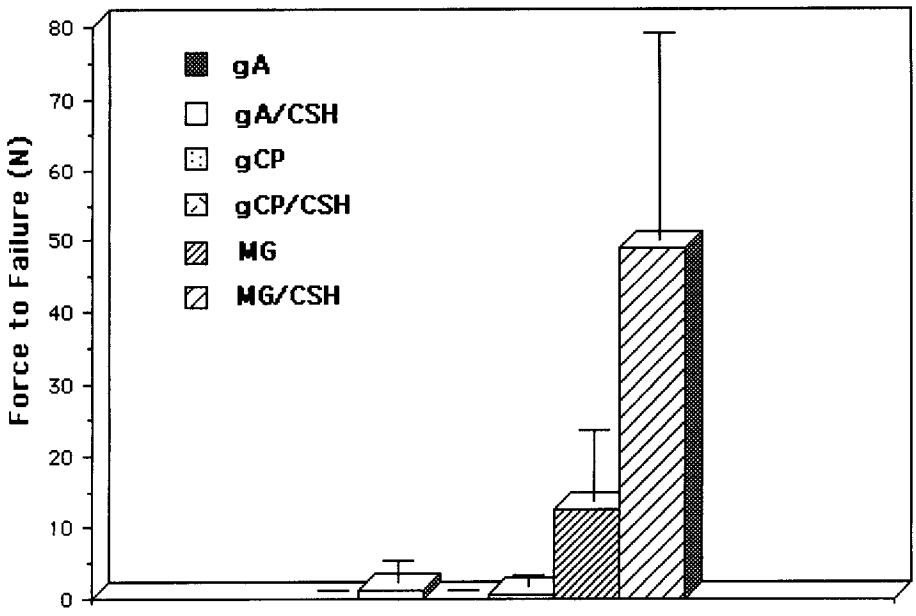

Figure 13. Graph of bone attachment strength (N) showing that only the MG12 and MG12/CS specimens showed measurable tensile attachment to bone. (From Ricci et al., in Bone Engineering, reprinted with permission.)



Figure 14. High power scanning electron micrograph of a deproteinated bone specimen from the IM rod study. The implant has been removed exposing ridges of bone mineral that had been in the microgrooves of the implant. Oriented openings left by cells are visible in the mineral structure. Bar = 10μm. (From Ricci et al., in Bone Engineering, reprinted with permission.)

Functional Biomaterials
doi:10.4028/www.scientific.net/KEM.198-199

Laser Microtexturing of Implant Surfaces for Enhanced Tissue Integration
doi:10.4028/www.scientific.net/KEM.198-199.179

click for feedback
consult - comment - contact
consult comment contact
click for feedback